Received 20 November 2020; revised 9 December 2020; accepted 10 December 2020. Date of publication 15 December 2020; date of current version 7 January 2021.

Digital Object Identifier 10.1109/OJCOMS.2020.3044680

Application-Based Coexistence of Different Waveforms on Non-Orthogonal Multiple Access

MEHMET MERT ŞAHIN [1] (Graduate Student Member, IEEE), AND HÜSEYIN ARSLAN[1,2] (Fellow, IEEE)

[1]Department of Electrical Engineering, University of South Florida, Tampa, FL 33620, USA

[2]Department of Electrical and Electronics Engineering, Istanbul Medipol University, 34810 Istanbul, Turkey

CORRESPONDING AUTHOR: M. M. ŞAHIN (e-mail: mehmetmert@usf.edu)

The work of Hüseyin Arslan was supported by the National Science Foundation under Grant ECCS-1609581.

ABSTRACT In the study, the coexistence of different waveform structures on the same resource element is studied under the theory of non-orthogonal multiple access (NOMA). This study introduces a paradigm-shift on NOMA towards the application-centric waveform coexistence. Throughout this article, the coexistence of different waveforms is explained with two specific use cases, which are power-balanced NOMA and joint radar-sensing and communication with NOMA. For the first use case, block error rate (BLER) performance in the power-balanced regime for two user is improved compared to conventional NOMA transmission with the same waveform. For the joint radar-sensing and communication aspect, the superiority of proposed NOMA scheme over orthogonal frequency division multiplexing (OFDM) joint radar-communication (JRC) scheme is demonstrated regarding radar ambiguity, channel estimation mean-square error (MSE) and bit-error rate (BER) performances. In addition, some of the previous works in the literature are reviewed regarding waveform coexistence in a non-orthogonal manner. However, the concept is not limited to these use cases. With the rapid development of wireless technology, next-generation wireless systems are proposed to be flexible and hybrid, having different kinds of capabilities such as sensing, security, intelligence, control, and computing. Therefore, the concept of different waveforms' coexistence to meet these concerns are becoming impressive for researchers.

INDEX TERMS FMCW, joint radar-sensing and communication, OFDM, OFDM-IM, waveform coexistence, waveform-domain NOMA.

I. INTRODUCTION

THE IDEA of serving multiple users in the same wireless resources, including frequency, time, code, and space, has become an appealing research area over almost thirty years. Efforts to investigate new types of multiple access techniques under the constraint of scarce resources are named as multi-user detection and non-orthogonal multiple access (NOMA) for decades. The main motivation behind NOMA having two different techniques, such as power-domain and code-domain, is the increased connectivity compared to orthogonal multiple access (OMA), which can meet the harsh requirements of the Internet of Things (IoT) [1]. Several NOMA schemes have been integrated into various standardization efforts. In LTE, the downlink NOMA scheme, called multi-user superposition transmission (MUST), was studied for the 3rd Generation Partnership Project (3GPP) Release 14 [2], whose motivation is weak in 5G, because higher performance gains can be provided with downlink massive multiple-input multiple-output (MIMO) [3]. A study on the application of NOMA for uplink transmission has been recently carried out for 3GPP Release 16, where different implementations of NOMA have been studied [4]. However, since power-domain NOMA has performance degradation in some cases, such as imperfect successive interference cancellation (SIC) and strict power control, it is not considered as a work-item in Release 17 [5].

On the other hand, the transmit power of users is arranged in a way that the users' power received at the base station (BS) is significantly different in order to enhance the overall system throughput in power-domain NOMA [6]. This

arrangement in power-domain NOMA introduces additional computational complexity that dynamically monitors the wireless system. Moreover, users transmitting at a similar power level may also be grouped in the case of high connectivity. Therefore, various researches have been conducted to find new NOMA schemes that operate in power-balanced scenarios [7].

With rapid developments in hardware such as large antenna arrays for millimeter wave (mmWave) and THz frequencies, efficient amplifiers, and ultra-capable digital signal processing (DSP) chips; and software regarding algorithms for detection and estimation capabilities, radar and communication systems tend to intersect in order to provide efficient usage of radio resources. Combining these two different worlds to work in harmony will pave the way for new techniques in wireless technologies that may enable lots of promising applications in wireless technologies to emerge [8]. For autonomous wireless networks, the capability to sense dynamically changing states of the environment and exchange information among various nodes needs to be integrated into 6G and beyond wireless systems [9]. Also, radar-sensing is seen as an enabling technology for environment-aware communication in 6G [10]. Therefore, this trend encourages both industry and academia to plan and use the available radio resources efficiently. For example, the WLAN sensing group is organized under the IEEE 802.11 study group [11], where techniques to utilize the existing Wi-Fi frame as a sensing node are being developed regarding the future use cases of the concept. As a result, these concerns have created the joint radar-sensing and communication concept, which has gained a significant amount of attention from both industry and academia [12]. So far, most of the papers investigate the optimal waveform to function jointly for both radar-sensing and communication, which is called joint radar-communication (JRC) waveform [13]. The aim is to combine radar-sensing and communication into a single mmWave system that utilizes a standard waveform. This kind of system is aimed to be optimized regarding cost, size, power consumption, spectrum usage, and adoption of communication-capable vehicles, for example, in case of autonomous driving, which needs both radar and vehicle-to-vehicle (V2V) communication [14].

The coexistence of Wi-Fi systems with other wireless technologies is an important issue needed to be solved intelligently [15]. Various methods are proposed to cover the coexistence of systems, including listen-before-talk mechanism, joint user association and resource allocation [16]. However, we introduce a novel concept on NOMA, which is the coexistence of different waveform structures in the same resource elements. This article studies two use cases of the introduced concept based on the superimposition of different waveforms non-orthogonally. The first use case is a power-balanced NOMA transmission scheme, which is presented by the authors in [17] where the OFDM and OFDM-IM waveforms are used in uplink transmission. Here, a downlink scenario of the proposed architecture is investigated with the calculation of achievable rates of the scheme. It is shown that when powers of users' signals are near to each other, the proposed scheme performs better compared to conventional power-domain NOMA with only orthogonal frequency division multiplexing (OFDM) waveform. The other use case is the implementation of the proposed NOMA concept including frequency modulated continuous-wave (FMCW) and OFDM waveforms in joint radar-sensing and communication, which is presented in [18]. The proposed NOMA scheme for the specific use case is compared with the existing OFDM JRC system presented in [19]. It is shown that proposed scheme outperforms in terms of both radar-sensing and communication functionality.

Contributions of this article can be listed as follows:

- A generalized method of different waveform coexistence with NOMA is introduced for application-based wireless networks.
- Two different use cases, which are power-balanced NOMA and joint radar-sensing and communication is studied in the view of waveform coexistence on the same resources.
- A novel power-balanced downlink NOMA transceiver design is proposed. The scheme is inspired by [17], where an uplink scheme is studied by authors. In this study, achievable rates of the proposed downlink scheme are calculated. Log-likelihood ratio (LLR) calculations are done to perform the separability and detectability of the signals. Effective block error rate (BLER) performance of the proposed NOMA scheme in the power-balanced regime is demonstrated by comparing to the conventional NOMA scheme with the same waveform.
- The superiority of the proposed NOMA scheme for joint radar-sensing and communication, which is firstly introduced in [18] by authors, is demonstrated in terms of ambiguity in radar-sensing functionality, channel estimation mean-square error (MSE) and bit-error rate (BER) performance by comparing with the existing OFDM JRC system proposed in [19].

The rest of this article is organized as follows: Section II summarizes the literature work related to waveform coexistence on NOMA. The power-balanced NOMA scheme, which is one of the use cases for waveform coexistence, is presented in Section III. Section IV introduces the use of waveform coexistence on NOMA in the field of joint radar-sensing and communication. Future possible studies and conclusions are drawn in Section V.

II. PREVIOUS WORKS

In this section, a few notable intelligent techniques proposed in the literature for the overlapping of users with different waveforms are presented. It is valuable to point out the definition of the waveform in wireless networks. The waveform consisting of symbol, pulse shape, and lattice is the physical shape of the signal carrying modulated information [28]. Any

TABLE 1. Existing literature works on waveform coexistence.

Coexisted Waveforms	Reference	Use case	Comments
OFDM + SC-FDMA	[20]	It can be used in LTE heterogeneous networks with overloaded users.	Both waveforms are used in LTE system. A novel multi-user detection (MUD) approach is proposed to separate waveforms.
OFDM + CDMA	[21]	It provides all users with the same data rate.	The proposed scheme relaxes the need for power allocation.
OFDM + OTFS	[22]	It offers flexibility among users considering their mobility profile.	Compared to OFDM, OTFS has a different lattice structure, where symbols are placed in delay-Doppler plane. OTFS-NOMA allows high mobility user to spread its signal over the whole time-frequency plane.
OFDM + OFDM-IM	[23], [24], [17]	It can be utilized in the power-balanced NOMA scenario and grant-free random access for URLLC	The OFDM-IM has some advantages over the OFDM such as ergodic achievable rate, PAPR reduction, and robustness to ICI [25], Therefore NOMA with OFDM and OFDM-IM introduces more flexible multiple access scheme regarding user's requirements.
OFDM + FMCW	[18]	It is designed for joint radar-sensing and communication functionality.	FMCW is a more suitable waveform for sensing purpose with condensed ambiguity function. The OFDM is utilized for communication purpose with high data-rate.
Multi-numerology OFDM-NOMA	[26]	Overloaded 5G networks can benefit from multi-numerology OFDM-NOMA.	Mixed numerologies are utilized against the constraints of MUD, as well as reduced guard duration.
MUSA with different Hermite-Gaussian prototype filters	[27]	It is proposed for 5G massive machine type communications (mMTC) service.	It increases the number of users by introducing third dimension, in addition to the time and frequency domains. In that dimension, symbols of users are spreaded by orthogonal Hermite-Gaussian functions.

change in the physical shape of signal is considered as a different waveform throughout this article. Therefore, the novel concept called coexistence of different waveforms proposes the superimposition of the signals with different physical shapes along over the non-orthogonal resources to introduce application-based flexibility, separability, and detectability. In Table 1, several previous works on different types of waveform coexistence are classified by pointing the aim behind such architectures.

In [21], a scheme based on non-orthogonally coexisting OFDM and code division multiple access (CDMA) is proposed. It is indicated that single-stage SIC achieves unsatisfactory performance under the presence of interference. Moreover, the power difference needed for SIC is compensated with the spreading nature of CDMA. The separability aspect on the overlapping of two different waveforms is investigated with an iterative receiver design that is computationally complex.

Similarly, the coexistence of OFDM and single carrier-frequency division multiple accessing (SC-FDMA) is studied in [20]. This work introduces a new degree of freedom to reuse the occupied radio resources by intentionally creating co-existence between different waveforms. It is shown that the proposed improved adaptive MUD approach utilizing iterative likelihood testing and signal to interference plus noise ratio (SINR) based processing outperforms conventional SIC.

Moreover, the orthogonal time frequency space (OTFS) waveform is used for the high mobility user, whereas the signal of the low mobility user is transmitted via the OFDM waveform in [22]. This OTFS-NOMA concept provides flexibility among users regarding their mobility profile. Reference [29] formulates the optimal beamforming design whose objective is to maximize the data rate of low-mobility NOMA users using OFDM, with the constraint that the requirement for high-mobility users' targeted data rate can be met.

Authors in [27] propose a novel multi-user shared access (MUSA) scheme with superimposing orthogonal waveforms whose filters are Hermite-Gaussian functions. These superimposed orthogonal functions introduce the third dimension in addition to time and frequency domains for each superimposed orthogonal functions. Here, the aim is to increase the total number of users that are served in the same resources. Besides high connectivity, the generalized frequency division multiplexing (GFDM) waveform is proposed to induce lower latency.

A NOMA scheme is proposed for the multi-numerology OFDM system in [26]. In the multi-numerology OFDM, which is common waveform family in 5G wireless networks, waveform structures differentiate with their lattice structure in time and frequency domain. The scheme utilizes the nature of mixed numerology OFDM systems to reduce the constraints associated with the multi-user detection (MUD) operation.

A novel downlink NOMA scheme with two users based on OFDM and OFDM with index modulation (OFDM-IM) is proposed in [23], called OFDM-IM NOMA. In this scheme, the inherent power imbalance of OFDM-IM leads to better throughput compared to conventional OFDM NOMA in the case of the power-balanced scenario. It is shown that OFDM-IM NOMA outperforms the classical OFDM NOMA in terms of BER under a total power constraint and achievable sum rate. The system performance of IM-NOMA is based on the power difference between the overlapped users as well as the inherent features of the OFDM-IM signal. This scheme is studied as grant-free access for uplink transmission, where multiple users are overloaded in the

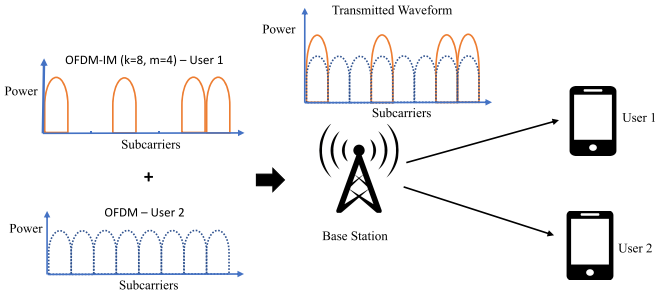

FIGURE 1. Two users downlink NOMA scheme with OFDM-IM+OFDM.

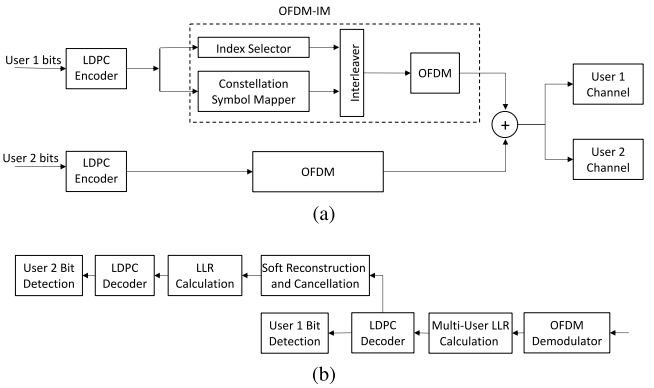

FIGURE 2. Proposed transmission and reception scheme (a) Coding and modulating of user 1 (OFDM-IM) and user 2 (OFDM) signals, (b) Demodulating and decoding of the superimposed received signal with LDPC codes aided soft reconstruction and cancellation.

same wireless communication resources [24]. It is proposed to reduce the effect of the collision on ultra-reliable and low-latency communications (uRLLC) services. Available resources are shared among the users when URLLC service is needed. K-repetitions transmission and maximum ratio combining (MRC) receiver are utilized to provide uRLLC service.

III. POWER-BALANCED NOMA TRANSMISSION

This section introduces the power-balanced NOMA scenario where waveform-domain NOMA scheme outperforms the classical NOMA scheme with the same waveform. The proposed downlink NOMA scheme including two different waveforms such as OFDM-IM and OFDM is compared with conventional OFDM-NOMA scheme in terms of the BER performance. In [30], BER analysis under the imperfect SIC based detection is evaluated with two user using OFDM-IM waveforms with different subcarrier allocation ratio and BER performance of single carrier frequency division multiple accessing (SC-FDMA) based index modulation (IM) scheme is studied in [31]. Also, it is well known that SIC based reconstruction and detection causes error propagation problem [32]. Therefore, the proposed scheme includes low-density parity-check (LDPC)-aided soft interference cancellation to diminish this problem. The use of this cancellation technique can be found in [17] where it is discussed for the uplink scenario. A transceiver design utilizing LDPC codes aided soft interference cancellation is presented to improve BLER performance when the received power of users are near to each other. The BLER performance may be improved through all received power level variations of users with more sophisticated coding schemes dedicated to the OFDM-IM waveform.

A. SYSTEM MODEL

For brevity, consider a two users downlink NOMA scenario in Fig. 1, where a single BS transmits the superimposed signal to both users over N subcarriers in the presence of frequency selective channels, including additive white Gaussian noise (AWGN). It is assumed that all transceivers are equipped with a single antenna. The transceiver architecture of the proposed NOMA scheme is presented in Fig. 2. The uplink scenario of the same scheme is investigated in the conference paper of the authors [17].

The LLR calculations are evaluated depending on the waveform type that is decoded first. It is shown that the proposed OFDM-IM and OFDM NOMA scheme outperforms the conventional power-domain NOMA scheme with OFDM waveform in terms of BLER performance in the power-balanced scenarios. Moreover, the proposed NOMA scheme provides flexibility among users regarding their demands.

B. CONVENTIONAL POWER-DOMAIN NOMA WITH OFDM+OFDM

Firstly, BS encodes messages of user equipments (UEs) by LDPC codes and modulate via quadrature amplitude modulation (QAM), where data symbols of users are drawn from a complex symbol alphabet $\mathbb{S}$. Then, these symbols are OFDM modulated and transmitted to be received by each UE over the same resource element (RE). Moreover, $p_{1,n}$ and $p_{2,n}$ denote the signal power of user 1 and user 2 at the nth subcarrier, respectively. In the OFDM with total N subcarriers, the total powers of user 1 and user 2 become $P_1 = \sum_{n=1}^{N} p_{1,n}$ and $P_2 = \sum_{n=1}^{N} p_{2,n}$, respectively. After the process of fast Fourier transformation (FFT) and removal of cyclic prefix, the baseband received signal at the nth subcarrier for each UE is expressed as follows:

$$r_{1,n} = h_{1,n}\left(\sqrt{p_{1,n}}u_{1,n} + \sqrt{p_{2,n}}u_{2,n}\right) + w_n, \qquad (1a)$$

and

$$r_{2,n} = h_{2,n}\left(\sqrt{p_{1,n}}u_{1,n} + \sqrt{p_{2,n}}u_{2,n}\right) + w_n, \qquad (1b)$$

where $h_{1,n}$, $h_{2,n}$, $u_{1,n}$, and $u_{2,n}$ are the channel gains and data symbols of users 1, and 2, respectively. Also, $w_n \sim \mathcal{CN}(0, \sigma^2)$ denotes the AWGN at the nth subcarrier.

Assuming that the signal of user 1 is decoded first where user 1 has more power, the capacity of user 1 (R_1) in conventional power-domain NOMA is given by

$$R_1 = \sum_{n=1}^{N} \log_2\left(1 + \frac{p_{1,n}h_{1,n}}{\sigma^2 + p_{2,n}h_{1,n}}\right) \text{ bit/s/Hz}. \qquad (2)$$

Assuming perfect SIC, which is infeasible, the capacity of user 2 (R_2) is calculated as follows:

$$R_2 = \sum_{n=1}^{N} \log_2\left(1 + \frac{p_{2,n}h_{2,n}}{\sigma^2}\right) \text{ bit/s/Hz}. \tag{3}$$

In the case of maximum likelihood multi-user detection (ML-MUD) without SIC, the decoding order does not have any effect on the sum-rate; therefore, any arbitrary decoding order can be assumed to be performed [33]. On the other hand, when maximum likelihood (ML)-MUD with SIC is used, the user with higher received power should be decoded first.

C. NOMA WITH OFDM-IM+OFDM

As Fig. 1 depicts, OFDM-IM waveform has been utilized for user 1, whereas OFDM waveform is used to send the signal of user 2 over N subcarriers. In the OFDM-IM scheme [34], the total $Q = Q_1 + Q_2$ bits are transmitted as follows: firstly, N subcarriers are split into total G subblocks consisting of k subcarriers. The Q_1 bits are used to determine the indices of m active subcarriers where the total number of active subcarrier positions is denoted as $c = Gm$. In each subblock β, only m out of k subcarriers have activated. Activated subcarriers are used to map Q_2 bits on to M-ary signal constellation symbols selected from the complex set $\mathbb{S}$. The information of user 1, which is carried in the subblock β, is given by $\mathbf{u}_{1,\beta} = [u_{1,\beta}^{(1)} \dots u_{1,\beta}^{(Q)}]$. Let Ω_j^β denote jth combination of the active subcarrier indices for subcarrier group β, whereas $\bar{\Omega}_j^\beta$ is the complement of it, including empty subcarriers at the β-th subgroup. As seen in Fig. 2(a), the interleaved grouping is performed to increase the achievable rate of OFDM-IM [35]. In subblock β, the vector of modulated symbols of user 2 carried with OFDM waveform is denoted by $\mathbf{u}_{2,\beta} = [u_{2,\beta}^{(1)} \dots u_{2,\beta}^{(k)}]$.

After FFT and cyclic prefix removal, the superimposed received signal for the users at the nth subcarrier becomes

$$r_{1,n} = h_{1,n}\left(\sqrt{\frac{kp_{1,n}}{mN}}u_{1,n} + \sqrt{p_{2,n}}u_{2,n}\right) + w_{1,n}, \tag{4}$$

$$r_{2,n} = h_{2,n}\left(\sqrt{\frac{kp_{1,n}}{mN}}u_{1,n} + \sqrt{p_{2,n}}u_{2,n}\right) + w_{2,n}, \tag{5}$$

where $u_{1,n} \in \mathbb{S}' = \{0, \mathbb{S}\}$. Moreover, denote $\mathbf{r}_\beta \in \mathbb{C}^{1\times k}$ as the received signal at the βth subgroup. Fig. 2(b) depicts the reception process of the proposed NOMA scheme by decoding the OFDM-IM waveform first. However, the decoding may not always start with the OFDM-IM waveform. It depends on both power, subcarrier allocation, and modulation order. When OFDM-IM waveform is removed first, the capacity analysis of the proposed NOMA scheme can be found in [23], whereas the other order of decoding is not studied there. In this article, capacity analysis of the scheme is evaluated when the OFDM waveform is removed first from the superimposed signal. Calculations for the capacity of users are performed on one subblock group. Assuming that the subcarriers in the subgroup are faded independently, the capacity of user 2 is written as

$$R_2 = \sum_{n\in\bar{\Omega}^\beta} \log_2\left(1 + \frac{p_{2,n}h_{2,n}}{\sigma^2}\right) + \sum_{n\in\Omega^\beta} \log_2\left(1 + \frac{p_{2,n}h_{2,n}}{\sigma^2 + \frac{kp_{1,n}}{mN}h_{2,n}}\right). \tag{6}$$

After successfully removing the OFDM signal from the superimposed signal, the capacity of user 1 with interleaved OFDM-IM waveform is lower bounded as follows [35]:

$$rClR_1 = \frac{m}{k}\log_2(M) + \frac{\log_2(C(k,m))}{k} - \frac{1}{C(k,m)kM^m} \times \sum_{j=1}^{C(k,m)}\sum_{m} \times \log_2\left(\sum_{j'=1}^{C(k,m)}\sum_{k-m}\frac{1}{\det\left(\mathbf{I}_k + \Lambda_{j,j'}\right)}\right), \tag{7}$$

where $C(k,m)$ denotes the binomial coefficient, $\mathbf{I}_k$ is the $k \times k$ unit matrix, $\Lambda_{j,j'}$ is an $k \times k$ diagonal matrix whose i-th diagonal element is given as

$$\left[\Lambda_{j,j'}\right]_{i,i} = \begin{cases} \frac{p_1 k}{2\sigma^2 m}\left|s_{t_{\Omega_j^{-1}(i)}} - s_{t'_{\Omega_j^{-1}(i)}}\right|^2, & i \in \Omega_j \cap \Omega_{j'}, \\ \frac{p_1 k}{2\sigma^2 m}\left|s_{t_{\Omega_j^{-1}(i)}}\right|^2, & i \in \Omega_j \cap \bar{\Omega}_{j'}, \\ \frac{p_1 k}{2\sigma^2 m}\left|s_{t'_{\Omega_j^{-1}(i)}}\right|^2, & i \in \bar{\Omega}_j \cap \Omega_{j'}, \\ 0, & i \in \bar{\Omega}_j \bigcap \bar{\Omega}_{j'}, \end{cases} \tag{8}$$

where $\mathbf{s}$ denotes the QAM modulated symbols in the activated m subcarriers, $\mathbf{s} = [s_{t_1}, \dots, s_{t_m}] \in \mathbb{S}^m$. As mentioned in [35], it should be noted that if $\Omega_j(r) = i$, then $\Omega_j^{-1}(i) = r \cdot \sum_{p^{(n)}} = \sum_{p_1=1}^{M} \dots \sum_{p_n=1}^{M}$. To conclude, (7) is the lower bound of the achievable data rate with interleaved OFDM-IM waveform for user 1.

D. LLR CALCULATIONS

This section includes the LLR calculations of each user for two different NOMA schees. Calculated LLRs are sent to the LDPC decoder as input. For the sake of fair comparison, we have used the log-sum approximation technique [36] to calculate approximate LLRs of two different NOMA schemes.

1) LLR CALCULATIONS FOR NOMA WITH OFDM+OFDM

With ML-MUD algorithm, the LLR of the bit i of user 1 at the nth subcarrier, $\Lambda_{n^{(i)}}^{u_1}$, is calculated as

$$\Lambda_{n^{(i)}}^{u_1} = \log\left(\frac{f\left(r_n | u_{1,n}^{(i)} = 0\right)}{f\left(r_n | u_{1,n}^{(i)} = 1\right)}\right) \approx \min_{u_{1,n}:\, u_{1,n}^{(i)}\in\mathbb{S}_1^i,\ u_{2,n}\in\mathbb{S}} \frac{\left\|r_n - h_{1,n}\left(u_{1,n} - u_{2,n}\right)\right\|^2}{\sigma^2} - \min_{u_{1,n}:\, u_{1,n}^{(i)}\in\mathbb{S}_0^i,\ u_{2,n}\in\mathbb{S}} \frac{\left\|r_n - h_{1,n}\left(u_{1,n} - u_{2,n}\right)\right\|^2}{\sigma^2}, \tag{9}$$

where $\mathbb{S}_b^i \subset \mathbb{S}$ denotes the set of all symbols $\alpha \in \mathbb{S}$ whose label has $b \in \{0, 1\}$ in bit position i. The complexity of this LLR calculation, in terms of complex multiplications, becomes $\sim O(|\mathbb{S}|^2)$. After LDPC decoder is fed with LLRs, the symbols of user 1 are reconstructed and subtracted from the superimposed signal with inevitable SIC error. The LLRs of user 2 are calculated with the remaining signal and sent to the LDPC decoder in order to obtain bit decisions of user 2.

2) LLR CALCULATIONS FOR NOMA WITH OFDMIM+OFDM

The LLR calculations for users' bits in the OFDM-IM+OFDM NOMA scheme depend on which waveform is decided to be decoded first. As it is shown via numerical results in Section III-E, the total power level is not the unique limitation to decide which waveform should be decoded first. By decoding the OFDM-IM waveform first, the LLR of the bit i of user 1 at the βth subgroup, $\Lambda_{\beta^{(i)}}^{u_1}$ is

$$\begin{aligned}\Lambda_{\beta^{(i)}}^{u_1} &= \log\left(\frac{f\left(\mathbf{r}_\beta | u_{1,\beta}^{(i)} = 0\right)}{f\left(\mathbf{r}_\beta | u_{1,\beta}^{(i)} = 1\right)}\right) \\ &\approx \min_{\mathbf{u}_{1,\beta}:\, u_{1,\beta}^{(i)}=1,\ \mathbf{u}_{2,\beta}\in\{S\}^k} \frac{\left\|\mathbf{r}_\beta - \mathbf{h}_{1,\beta} \odot \left(\mathbf{u}_{1,\beta} - \mathbf{u}_{2,\beta}\right)\right\|^2}{\sigma^2} \\ &\quad - \min_{\mathbf{u}_{1,\beta}:\, u_{1,\beta}^{(i)}=0,\mathbf{u}_{2,\beta}\in\{S\}^k} \frac{\left\|\mathbf{r}_\beta - \mathbf{h}_{1,\beta} \odot \left(\mathbf{u}_{1,\beta} - \mathbf{u}_{2,\beta}\right)\right\|^2}{\sigma^2},\end{aligned} \tag{10}$$

where $\mathbf{h}_{1,\beta} \in \mathbb{C}^{1\times k}$ and $\mathbf{h}_{2,\beta} \in \mathbb{C}^{1\times k}$ denote the channel state information (CSI) of users 1 and 2 through βth subgroup, respectively, and $\odot$ denotes Hadamard multiplication. When the OFDM-IM waveform is decoded first, the complexity of LLR calculation, in terms of complex multiplications, becomes $\sim O(c|\mathbb{S}|^m|\mathbb{S}|^k)$. On the other hand, starting the decoding process with the OFDM waveform, the LLR of the bit i of user 2 at the nth subcarrier, $\Lambda_{n^{(i)}}^{u_2}$, becomes

$$\begin{aligned}\Lambda_{n^{(i)}}^{u_2} &= \log\left(\frac{f\left(r_n | u_{2,n}^{(i)} = 0\right)}{f\left(r_n | u_{2,n}^{(i)} = 1\right)}\right) \\ &\approx \min_{u_{2,n}:\, u_{2,n}^{(i)}\in\mathbb{S}_1^i,\ u_{1,n}\in\mathbb{S}'} \frac{\left\|r_n - h_{2,n}\left(u_{2,n} - u_{1,n}\right)\right\|^2}{\sigma^2} \\ &\quad - \min_{u_{2,n}:\, u_{2,n}^{(i)}\in\mathbb{S}_0^i,\ u_{1,n}\in\mathbb{S}'} \frac{\left\|r_n - h_{2,n}\left(u_{2,n} - u_{1,n}\right)\right\|^2}{\sigma^2}.\end{aligned} \tag{11}$$

By decoding the OFDM waveform first, the complexity of the LLR calculation, in terms of complex multiplications, becomes $\sim O(|\mathbb{S}'||\mathbb{S}|)$. The waveform, whichever is decoded first, is reconstructed and subtracted from the aggregate received signal before the next user's signal is decoded.

E. NUMERICAL EVALUATION

The proposed technique is evaluated numerically through Monte Carlo simulations. As in [21], the performance of the proposed NOMA scheme is evaluated with BLER metric. Since the SIC is not perfectly performed in practice, achievable rate analysis under the perfect SIC condition misleads the comparison of the schemes. As for the modulation order, QPSK signaling is used for both NOMA schemes, where equal data rate is satisfied with three active subcarriers in groups of four subcarriers ($m = 3$, $k = 4$) for the user utilizing the OFDM-IM waveform. For OFDM+OFDM NOMA, two different decoding schemes are investigated called ML and ML-SIC. For the ML-SIC based decoding, the user with high received power is decoded first, then reconstructed, and eliminated from the superimposed signal, whereas users' bits is directly demodulated with ML algorithm in the ML based decoding. On the other hand, for OFDM-IM+OFDM NOMA, the decoding order is determined according to waveform type. Firstly decoded waveform is shown as bold for all given plots.

Fig. 3(a) and Fig. 3(b) demonstrate the performance of conventional OFDM NOMA and proposed OFDM-IM NOMA schemes over the frequency selective channel with 10 taps for user 1 and user 2, respectively. Code rate is selected as 0.5 with 256 block length. Throughout the simulation, it is assumed that channel knowledge is present at the receiver.

The vertical axis denotes the required signal-to-noise ratio (SNR) for a user to achieve the target BLER of 1‰, whereas the horizontal axis denotes the power difference in terms of dB between two different users. OFDM-IM+OFDM NOMA is superior in terms of BLER at the region, where power difference between users is very close to 0 dB. However, as power imbalance between the users is close to each other in conventional OFDM NOMA, the performance degrades significantly because power coefficients of the users equate the aggregated signal to the decision boundary. These regions are called as ambiguity region where user's messages are not decoded even with high SNR. As opposed to conventional power-domain NOMA, the superior region of the user 1 and user 2 in the proposed scheme is roughly below 2 dB and above -2 dB, respectively. Due to inherent power imbalance in OFDM-IM, the decision of symbol is perplexed when aggregate symbol falls into decision boundary at the 5 dB power imbalance. Nevertheless, ambiguity region can not be seen in the proposed scheme by decoding OFDM-IM first, it can be decoded at roughly 20 dB with the help of null subcarriers in OFDM-IM waveform. Using forward error correction with soft reconstruction and cancellation removes deep performance losses in the range of certain power differences for OFDM-IM+OFDM NOMA scheme. However, conventional power-domain NOMA still has a region where the performance degrades significantly. The proposed waveform-domain NOMA scheme is superior at the region where the power of users is close to each other without having

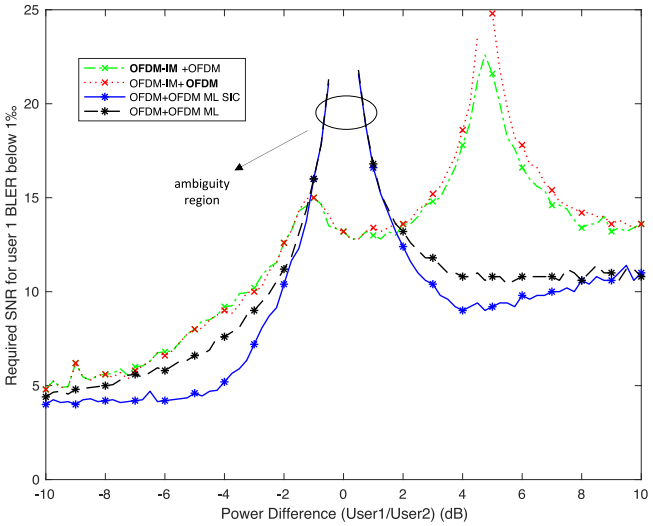

(a)

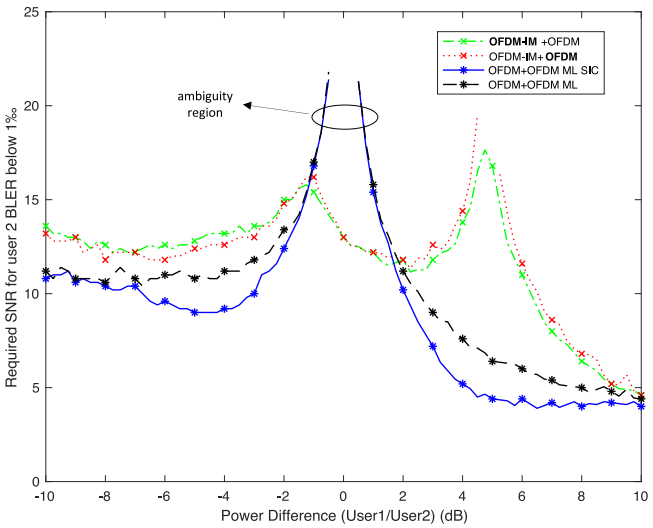

(b)

FIGURE 3. Comparison of proposed waveform-domain NOMA and conventional OFDM-OFDM NOMA in downlink transmission, (a) BLER of user 1, (b) BLER of user 2.

significant performance losses as the power difference between users increases.

IV. JOINT RADAR-SENSING AND COMMUNICATION FRAMEWORK WITH NOMA

Joint radar-sensing and communication can be actualized using different approaches such as frequency-sharing, time-sharing and signal-sharing [37]. Time and frequency sharing approaches can be regarded as resource scheduling in wireless systems. Scheduling techniques make efficient use of hardware, but limit the spectral efficiency. On the other hand, the main aim of the signal-sharing approach is to have one waveform performing both functions, i.e., data embedded radar waveform or communication waveform with radar capabilities including multi or single carrier systems [38]. The use of waveform-domain NOMA scheme superimposing

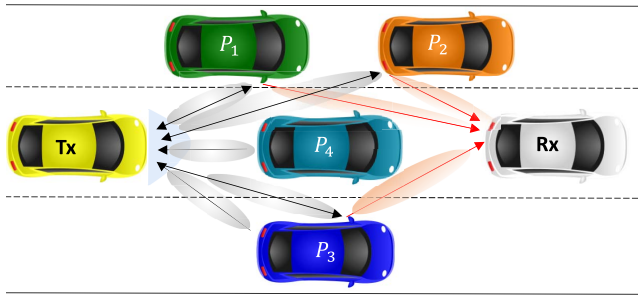

(a)

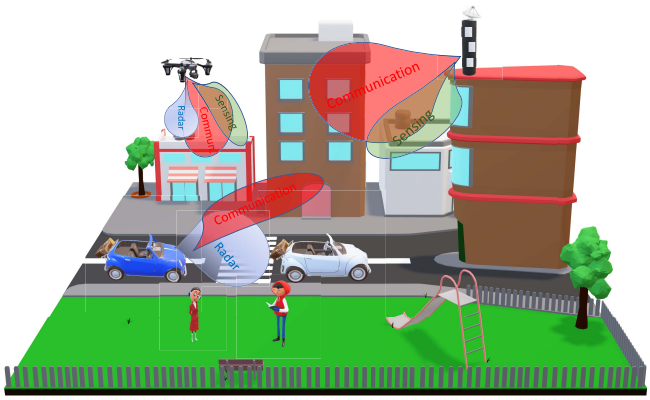

(b)

FIGURE 4. System model needing both radar-sensing and communication functionality, (a) V2V joint radar-communication, (b) generalized framework for joint radar-sensing and communication.

FMCW and OFDM waveforms to support joint radar-sensing and communication is firstly proposed by authors in [18]. Here, the superiority of the proposed NOMA scheme over the conventional OFDM scheme for JRC [19] is demonstrated. The proposed architecture separately performs radar-sensing and communication functions using the same radio resources non-orthogonally and leverages the information obtained from radar process to the communication functionality.

A. SYSTEM MODEL

The V2V scenario is considered as shown in Fig. 4(a), however, the proposed scheme is also applicable for different use cases needing both radar-sensing and communication activity. For example, more complicated wireless network system is shown in Fig. 4(b), including several nodes that function both radar-sensing and communication The general transmission and reception scheme can be seen in Fig. 5 where radar-sensing knowledge obtained from FMCW is leveraged to perform the channel estimation process in OFDM waveform.

B. TRANSMISSION DESIGN

The FMCW waveform consisting of many chirps and the OFDM waveform are utilized for radar-sensing and communication operations, respectively. The complex equivalent time-domain representation of one chirp, whose frequency

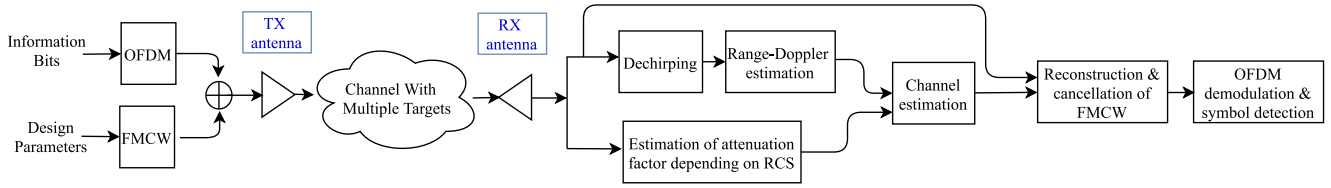

FIGURE 5. Transmission and reception operations of the proposed NOMA scheme for joint radar-sensing and communication.

increases linearly across a total bandwidth of β Hz during the τ-second is expressed as [39]

$$s_{\text{chirp}}(t) = e^{j\pi\beta t^2/\tau}, \quad 0 \le t \le \tau. \tag{12}$$

The FMCW waveform consisting of K chirps per frame is

$$s_{\text{FMCW}}(t) = \sqrt{P_{\text{FMCW}}} \sum_{k=0}^{K-1} s_{\text{chirp}}(t - k\tau), \quad 0 \le t \le T, \tag{13}$$

where T and P_{FMCW} denote the total frame duration and power of the FMCW waveform, respectively.

Let $\{d_n\}_{n=0}^{N-1}$ be the complex symbols modulated via QAM drawn from a complex symbol alphabet $\mathbb{S}$. An OFDM symbol with N subcarriers is expressed in the time-domain as follows:

$$s_{\text{OFDM}}(t) = \sqrt{P_{\text{ofdm}}} \sum_{n=0}^{N-1} d_n e^{j2\pi n\Delta f t}, \quad 0 \le t \le T_s, \tag{14}$$

where T_s, Δf and P_{OFDM} denote one OFDM symbol duration, the subcarrier spacing and the OFDM power, respectively.

A cyclic prefix (CP) of length T_g is prepended to each OFDM symbol to keep OFDM subcarriers orthogonal by preventing inter-symbol interference (ISI) across OFDM symbols. The CP transforms the linear convolution of the multipath channel to a circular convolution, where one-tap equalization can be used [40]. After the CP addition, the mth OFDM symbol can be expressed as

$$\bar{s}_m(t) = \begin{cases} s_{\text{OFDM}}\big(t + T_s - T_g\big), & \text{if } 0 \le t \le T_g, \\ s_{\text{OFDM}}\big(t - T_g\big), & \text{if } T_g < t \le T_{\text{OFDM}}, \end{cases} \tag{15}$$

where $T_{\text{OFDM}} = T_g + T_s$ is the duration of one OFDM symbol after CP addition. Having M OFDM symbols in a frame during $T_{\text{sym}} = T - \tau$, the time-domain OFDM signal can be represented as follows:

$$\bar{s}_{\text{OFDM}}(t) = \sum_{m=0}^{M-1} \bar{s}_m(t) \times \text{rect}\left(\frac{t - mT_{\text{OFDM}}}{T_{\text{OFDM}}}\right), \quad 0 \le t \le T_{\text{sym}}. \tag{16}$$

In the proposed NOMA scheme, the transmitted frame $s(t)$ superimposes both waveforms. To obtain the radar cross section (RCS) information of the objects in the environment, single chirp is prepended to the NOMA frame. The final transmit frame for the objectives of multi-functional radar-sensing and communication transmission is designed as follows:

$$s(t) = \begin{cases} s_{\text{FMCW}}(t), & \text{if } 0 \le t \le \tau, \\ s_{\text{FMCW}}(t) + \bar{s}_{\text{OFDM}}(t), & \text{if } \tau < t \le T. \end{cases} \tag{17}$$

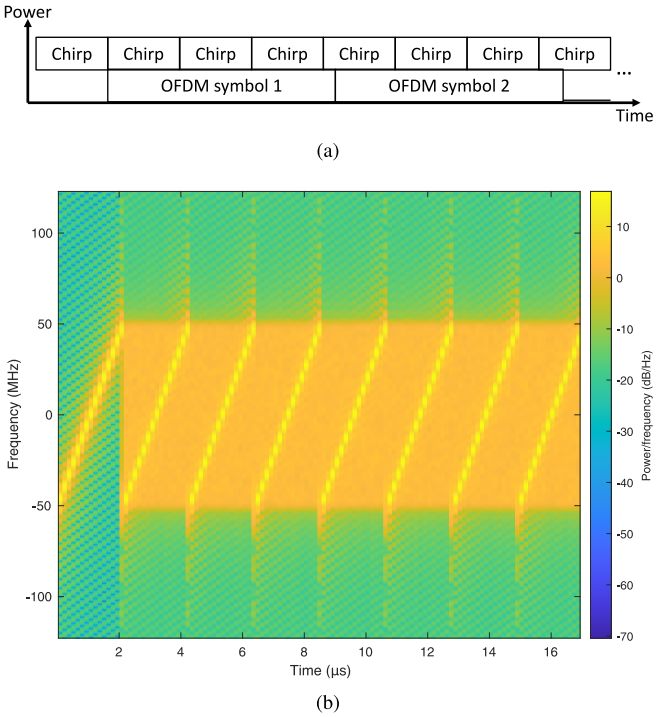

FIGURE 6. Proposed transmitted NOMA frame for joint radar-sensing and communication functionality, (a) time-power representation, (b) time-frequency representation.

The transmitted frame can be seen in Fig. 6(a) where it starts with a chirp following the superimposed OFDM symbols and many chirps. The waveforms are superimposed in a way that the allocated bandwidth is the same for each waveform type. The time-frequency illustration of the superimposed signal can be seen in Fig. 6(b). It can be realized that the OFDM signal is distributed along with the whole bandwidth, whereas FMCW waveform patterns consecutive pulses whose frequency increases linearly. It should be noted that there is power leakage in frequency band in the case of transition from one waveform to another. It can be reduced with proper windowing operations, however, it is beyond the scope of this article.

Then, the baseband signal $s(t)$ is upconverted to the desired radio frequency (RF) band, where the transmitted

passband analog signal becomes

$$x(t) = \Re\left\{s(t)e^{j(2\pi f_c t+\bar{\theta})}\right\}, \tag{18}$$

where $\Re\{.\}$ denotes the real part of the complex quantity. The notations f_c and $\bar{\theta}$ are the carrier frequency and the initial phase of the transmitted signal, respectively.

C. CHANNEL EFFECT

The Doppler shift due to mobility and flight time for the paths reflecting from the targets are as shown in Fig. 4(a). It is assumed that the environment does not change over a coherent transmission time T leading to fixed Doppler shifts and delays. Actually, it is a reasonable assumption that is commonly used in radar literature [39]. With modeling the environment that signal propagates as a linear time-varying channel [41], the received passband signal is represented as follows:

$$r(t) = \sum_{p=1}^{P} \alpha_p \Re\left\{x\big(t-\tau_p\big)e^{j2\pi(f_c+\psi_p)(t-\tau_p)}\right\} + n(t), \tag{19}$$

where α_p and τ_p are the attenuation factor depending on non-fluctuating radar cross section (RCS) and time delay related with the distance between the transmitter to target plus target to the receiver (bi-static range) for the p target, respectively. There exist total P target in the environment causing signal reflections, in other words, P is the number of specular scatterers. The notation $\psi_p = \frac{f_c \upsilon_p}{c}$ is the Doppler frequency associated with the pth path depending on relative speed υ_p and the speed of light c. Also, $n(t) \sim \mathcal{CN}(0, \sigma^2)$ denotes the additive AWGN. The attenuation factor α_p is proportional to the large-scale path-loss. Having the path distance d between receiver and transmitter, the large-scale path-loss G is given as

$$G = \frac{G_{\mathrm{TX}} G_{\mathrm{RX}} \lambda^2}{(4\pi)^2 d^{\mathrm{PL}}}, \tag{20}$$

where PL is the path-loss exponent, G_{TX} and G_{RX} are the transmit and receive antenna gain, respectively.

D. MULTI-FUNCTIONAL RECEPTION

In this section, the receiver scheme for radar-sensing and communication operations is investigated. Since the receiver performs both functions, the knowledge obtained from one process can be leveraged to another to improve the performance.

1) BI-STATIC RADAR FUNCTIONALITY AND CHANNEL ESTIMATION

Down-converting the received passband signal $r(t)$ into baseband and sampling with the frequency of $F_s = N\Delta f$, the discrete-time signal becomes

$$y[n] = \sum_{p=1}^{P} h_p x\big(n/F_s - \tau_p\big)e^{j2\pi n\psi_p/F_s} + w(n), \;\; n \in \mathbb{N}^+, \tag{21a}$$

and

$$h_p = \alpha_p e^{-j2\pi(f_c+\psi_p)\tau_p + j\bar{\theta}}, \tag{21b}$$

where h_p is the complex channel gain of pth target and $\bar{\theta}$ is the phase error. Then, the stretch processing is employed in the discrete domain for the superimposed signal to get delays and Doppler shifts estimations. The processed signal in one chirp time interval can be written as

$$\bar{y}\big[n'\big] = y\big[n'\big] \times e^{-j\pi\beta(n'/F_s)^2/\tau}, \quad n' = 1, 2, \ldots, \lfloor \tau F_s \rfloor = N_c, \tag{22}$$

and dechirping process is repeated for each chirp time interval. Remember that stretch processing is generally done in time domain with down-conversion. However, here it is assumed that the occupied bandwidth of FMCW is the same as OFDM bandwidth, therefore, the sampling rate F_s for both radar and communication is taken as equal to each other.

The fast-time/slow-time coherent processing interval (CPI) matrix $\mathbf{K} \in \mathbb{C}^{K \times N_c}$ is formed where fast time samples (l) are obtained at the rate of F_s from the points on each chirp. Slow-time samples (k) are taken from the points on every chirp at the same fast-time sample point. Then this matrix is utilized to perform periodogram based radar processing. The output power of the periodogram at the mth Doppler and nth range bin is

$$P(m,n) = \frac{1}{KN_c}\underbrace{\left|\sum_{k=0}^{N_c-1}\left(\overbrace{\sum_{l=0}^{K-1}(\mathbf{K})_{k,l}e^{-j2\pi\frac{lm}{K}}}^{N_c\,\mathrm{FFT}_{\mathrm{soflength}\,K}}\right)e^{-j2\pi\frac{kn}{N_c}}\right|^2}_{K\,\mathrm{FFT}_{\mathrm{soflength}\,N_c}}, \tag{23}$$

sinusoids in $\mathbf{K}$ related to object's distance and velocity lead to peaks in $P(m, n)$. Then certain distance and velocity values can be found from related range and Doppler bin value of peaks.

Estimation of complex attenuation factor h_p for every pth scatterer (target) is done with the first chirp by the least-square estimation [42]. It is worth to note that first chirp in the transmitted frame is interference-free as seen in Fig. 6(a). Let the vector $\mathbf{y_c} \triangleq [y[1], y[2], \ldots, y[\tau F_s]]^{\mathrm{T}}$ be the samples of the received signal throughout the time τ, the estimated complex attenuation coefficients $\hat{\mathbf{h}} \triangleq [\hat{h}[1], \hat{h}[2], \ldots, \hat{h}[P]]^{\mathrm{T}}$ become

$$\hat{\mathbf{h}} = \arg\min_{\mathbf{h}} (\mathbf{y_c} - \mathbf{B}\mathbf{h})^H (\mathbf{y_c} - \mathbf{B}\mathbf{h}), \tag{24}$$

where $\mathbf{B}$ is a $(\tau F_s - \bar{n}) \times P$ matrix whose rows corresponds to different shifts of the transmitted chirp where shift values are determined according to the estimated range value of the pth scatterer (target). The offset value $\bar{n} \in \mathbb{N}$ depends on the maximum range requirement of the system. Also, the selection of higher value for $\bar{n}$ decreases fluctuations in the estimation of $\hat{\mathbf{h}}$ depending on Doppler shifts along with one chirp, whereas the maximum range is reduced. By

differentiating with respect to $\mathbf{h}$ and setting the result equal to zero, the least-square estimation of the channel becomes

$$\hat{\mathbf{h}} = \left(\mathbf{B}^H\mathbf{B}\right)^{-1}\mathbf{B}^H\mathbf{y}. \tag{25}$$

Besides the estimation of delays τ_p and Doppler shifts ψ_p, the matrix $\hat{\mathbf{h}}$ completes the process to recreate the channel matrix $\mathbf{H}$ with some estimation errors.

2) COMMUNICATION FUNCTIONALITY

Here, the communication symbols are demodulated using the estimated channel knowledge in the previous section. Let the channel gain of the kth sample of the transmitted signal during the reception of the nth sample denote as $h_{n,k}$. Also, if the discrete channel convolution matrix along one OFDM symbol duration with N_{OFDM} samples is shown as $\mathbf{H} \in \mathbb{C}^{(N_{\text{OFDM}})\times(N_{\text{OFDM}})}$, the element in the kth column of the nth row of $\mathbf{H}$ is $h_{n,k}$. Firstly, the FMCW sequence is removed from the total received signal by using estimated channel matrix $\hat{\mathbf{H}}$ as follows:

$$\mathbf{y}_{\text{OFDM}} = \mathbf{y} - \hat{\mathbf{H}}\mathbf{s}_{\text{FMCW}}, \tag{26}$$

where $\mathbf{y}_{\text{OFDM}} = [\mathbf{y}_1, \mathbf{y}_2, \ldots, \mathbf{y}_M]$ and $\mathbf{y}_m$ is the mth OFDM symbol in the received vector $\mathbf{y}$. The CP addition matrix $\mathbf{A} \in \mathbb{R}^{N_{\text{OFDM}}\times N}$ is defined as

$$A = \begin{bmatrix} \mathbf{0}_{N_g\times N} & \mathbf{I}_{N_g} \\ & \mathbf{I}_{\mathbf{N}_{\text{OFDM}}} \end{bmatrix}, \tag{27}$$

and the CP removal matrix is generated as $\mathbf{B} = [\mathbf{0}_{N\times N_g}\mathbf{I}_N]$ where N_g is the total sample number during CP duration T_g. The matrix $\hat{\Theta} \in \mathbb{C}^{N\times N}$ is the estimated channel frequency response (CFR) matrix which equals to

$$\hat{\Theta} = \mathbf{F}_N\mathbf{B}\hat{\mathbf{H}}\mathbf{A}\mathbf{F}_N^{\text{H}}. \tag{28}$$

The diagonal components of (28) are the channel coefficients scaling the subcarrier in interest collected in a vector $\hat{\boldsymbol{\theta}} = \text{diag}\left(\hat{\Theta}\right)$. Off-diagonal components of $\hat{\Theta}$ are not zero due to Doppler effect from the channel causing inter-carrier interference (ICI). Finally, estimates of QAM data symbols for mth OFDM symbol are obtained as:

$$\hat{\mathbf{d}_m} = \left(\left(\text{diag}\left(\hat{\boldsymbol{\theta}} \odot \hat{\boldsymbol{\theta}}^*\right)\right)^{-1}\text{diag}\left(\hat{\boldsymbol{\theta}}\right)^*\mathbf{F}_N\mathbf{B}_K\mathbf{y}_m\right), \tag{29}$$

where $\text{diag}\left(\hat{\boldsymbol{\theta}}\right)$ returns a square diagonal matrix with the elements of vector $\hat{\boldsymbol{\theta}}$ on the main diagonal. This equation finalizes the proposed receiver structure without introducing pilots on the OFDM subcarriers to estimate the channel.

E. NUMERICAL EVALUATION OF THE PROPOSED NOMA SCHEME

In this section, the radar-sensing and communication performance of the proposed NOMA scheme is compared with the OFDM scheme with pilots for JRC systems proposed in [19]. Comb-type pilot design is used for the compared scheme and pilot spacings in frequency (D_f) and time (D_t) is arranged as follows [43]:

$$D_f \leq \frac{1}{\tau_{\max}\Delta f}, \tag{30a}$$

and

$$D_t \leq \frac{1}{2f_{d_{\max}}T_{\text{sym}}}, \tag{30b}$$

where $f_{d_{\max}}$ and $\tau_{\max}$ denote the maximum Doppler shift and delay caused by targets, respectively. To satisfy the constraints given in (30a) and (30b), QPSK modulated Gold sequences [44] are inserted into one in every four subcarriers for each OFDM symbol. Simulation parameters for proposed NOMA scheme depending on radar and communication requirements are shown in Table 2. It is assumed that the maximum delay $\tau_{\max}$ is smaller than the CP length of each OFDM symbol and the channel includes three targets in the bi-static radar case, as shown in Fig. 4(a). The power delay profile (PDP) of the channel is determined as an exponentially decaying function where the power of channel coefficients is set as $\text{E}\,[h_p(\gamma)]^2 = \eta e^{-\gamma p}$, where η denotes the normalization factor and p is the target index. The decaying factor γ is taken as unity for simplicity and each tap amplitude follows Rayleigh distribution. During the simulation, powers of waveforms P_{OFDM} and P_{FMCW} equal to each other. However, the distribution of power between FMCW and OFDM can be arranged according to system requirements for each chirp and OFDM symbol. Then, it turns out a optimization problem with constraints of data rate and Cramér-Rao lower bound (CRLB) of parameter estimation for communication and radar-sensing functionalities, respectively.

TABLE 2. Simulation parameters.

Parameter	Value
Carrier frequency (f_c)	28 GHz
Bandwidth (β)	122.88 MHz
Chirp duration (T_c)	2.4 µs
Number of chirps (T_c)	640 µs
Duration of proposed NOMA scheme (T)	2.8 ms
Subcarrier spacing(Δf)	60 kHz
Number of FFT(N)	2048
Range of targets	15 m, 90 m and 180 m
Relative velocity of targets	0 m s^{-1}, 23.2 m s^{-1} and −30.9 m s^{-1}

The comparison of radar-sensing performance of proposed NOMA scheme and OFDM JRC is depicted in Fig. 7 when the SNR of the transmitted signal is 10 dB. For both scheme, periodogram based estimation is utilized which is explained in (23). As it can be seen in Fig. 7(a), three different reflections can be identified clearly, whereas OFDM JRC scheme includes side-lobes seen in Fig. 7(b) which deteriorates the radar detection performance. Side-lobes in the periodogram of OFDM JRC scheme results from the copies of the existing targets beyond the unambiguous radar range due to fixed placement of pilots.

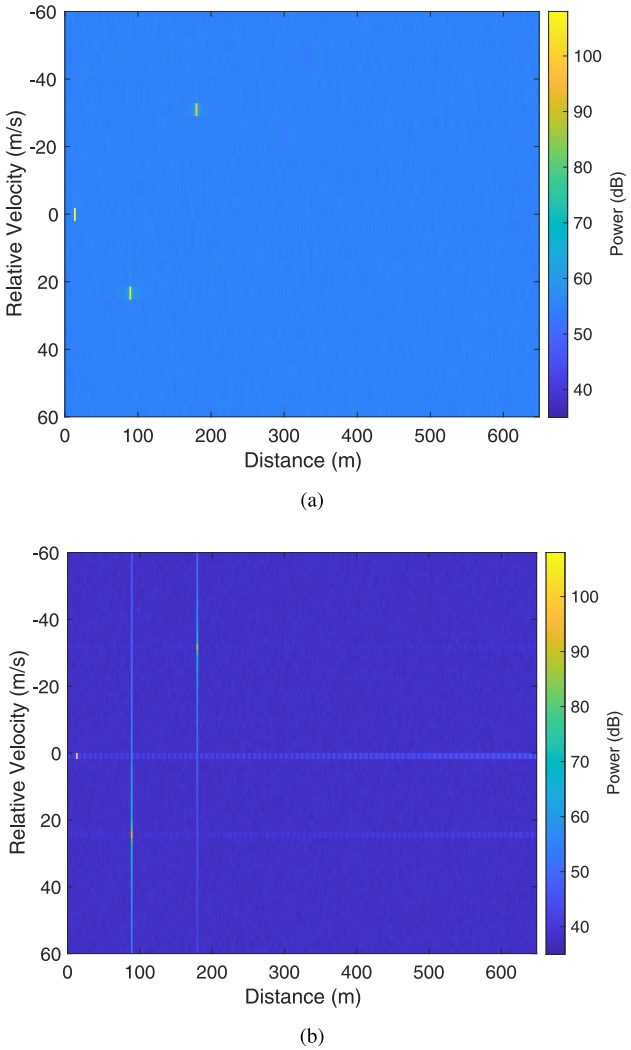

FIGURE 7. Radar detection performance comparison via periodogram method where SNR equals to 10 dB (a) proposed NOMA scheme (b) conventional OFDM scheme with comb-type pilot structure.

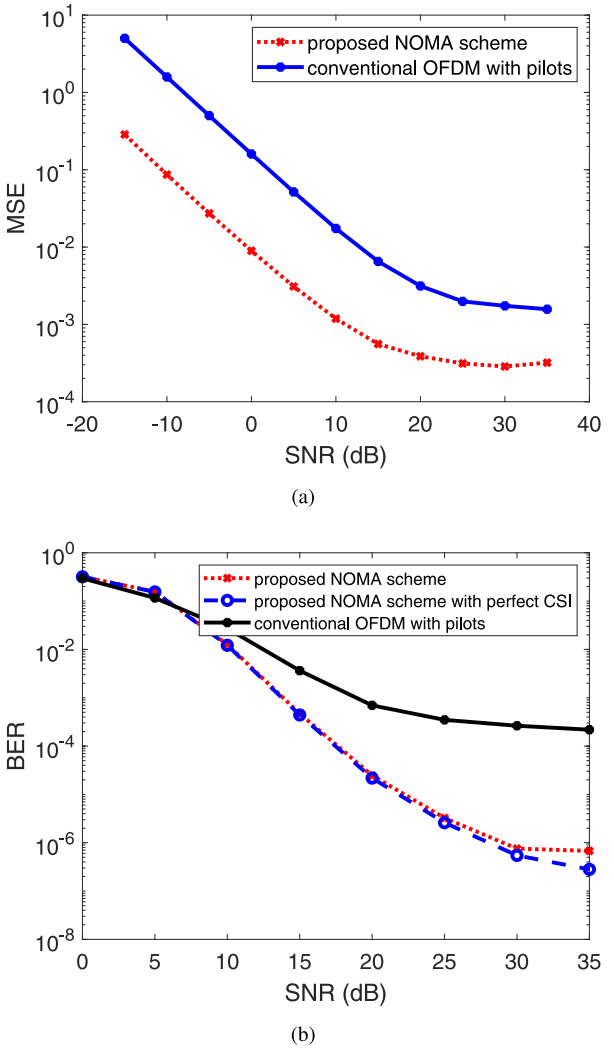

FIGURE 8. Performance evaluation of proposed method (a) distance-velocity plot of the targets where SNR equals to 20 dB (b) BER performance of proposed method.

MSE is calculated considering diagonal elements of $\hat{\boldsymbol{\Theta}}$ presented in (28) and its true value $\boldsymbol{\Theta}$. The MSE is represented as $\sigma_e^2 = \frac{\mathrm{E}[|\hat{\boldsymbol{\theta}}-\boldsymbol{\theta}|^2]}{\mathrm{E}[|\boldsymbol{\theta}|^2]}$, where $\mathrm{E}[\cdot]$ denotes the expected value. Channel estimation process of conventional OFDM JRC scheme is performed with transform domain technique [43]. First, the CFR vector is obtained by implementing spline interpolation over pilots. Then, IFFT of the CFR is taken. The resultant transform domain is the time domain, where typically the channel taps are concentrated into a sub-region. By zeroing the terms out of this sub-region that corresponds to noise only, the significant taps are obtained. This sub-region is determined via the length of CP. The noise reduced signal is then transformed back into the frequency domain via FFT operation to retain $\hat{\boldsymbol{\theta}}$. MSE performance of the proposed NOMA scheme and OFDM JRC can be seen in Fig. 8(a), which degrades as SNR increases. Proposed NOMA scheme performs well beyond the OFDM JRC. It is worth noting that the complex attenuation factors for each target are estimated using the first chirp, while delays and Doppler shifts are estimated using the FMCW waveform in the proposed NOMA scheme. After evaluating the complex attenuation factor h_p denoted in (21b), the estimation of channel matrix $\hat{\mathbf{H}}$ is created by using the obtained values of Doppler shifts and delays which is done previously via FMCW waveform. Finally, this channel estimation is used to demodulate communication symbols in the OFDM waveform.

The BER performance of the proposed NOMA scheme, where channel estimation knowledge is leveraged from the FMCW waveform, can be seen in Fig. 8(b) by comparing it with OFDM JRC. The information bits are encoded via 1/2 rate convolutional codes with interleaving to get rid of the deep fading effect of the channel. The proposed NOMA scheme is also compared with the presence of perfect CSI. In other words, the FMCW waveform is totally removed from the superimposed signal without affecting the OFDM waveform and OFDM signal is demodulated with perfect

channel estimation. Proposed NOMA scheme outperforms the conventional OFDM JRC scheme proposed in [19] which reaches error floor after 25 dB due to multiple Doppler shifts in the channel. It can also be seen that performance degradation of the proposed NOMA scheme is negligible compared to case where perfect CSI is available. It should be noted that, ICI effect is not totally removed and demodulation is performed as it is shown in (29). To sum up, non-orthogonally coexistence of two different waveforms, OFDM and FMCW, has good sensing accuracy with minimal degradation to communication performance.

V. CONCLUSION

This article aims to introduce the concept called application-based waveform-domain coexistence on NOMA to meet wide variety of applications proposed in 5G, 6G and beyond wireless networks. The concept emanates from the waveform-domain NOMA principle proposed by the authors where different waveforms are superimposed over the available radio resources. Two main applications of the concept is introduced throughout this article which are the power-balanced NOMA and joint radar-sensing and communication based on waveform domain NOMA. These approaches clearly indicate the use cases of the concept, however, variation of waveforms regarding applications of wireless networks can be extended. Since the coexistence of different waveforms serves the need of flexibility considering applications and use cases that future wireless systems offers, it is likely that researchers pay attention to improve practicability of the proposed NOMA concept.

REFERENCES

[1] Z. Ding *et al.*, "Application of non-orthogonal multiple access in LTE and 5G networks," *IEEE Commun. Mag.*, vol. 55, no. 2, pp. 185–191, Feb. 2017.

[2] "Study on downlink multiuser superposition transmission (MUST) for LTE, version 13.0.0," 3GPP, Sophia Antipolis, France, Rep. 36.859, Jan. 2016.

[3] Y. Yuan, Z. Yuan, and L. Tian, "5G non-orthogonal multiple access study in 3GPP," *IEEE Commun. Mag.*, vol. 58, no. 7, pp. 90–96, Jul. 2020.

[4] "Study on non-orthogonal multiple access (NOMA) for NR, version 13.0.0," 3GPP, Sophia Antipolis, France, Rep. 38.812, Dec. 2018.

[5] B. Makki, K. Chitti, A. Behravan, and M.-S. Alouini, "A survey of NOMA: Current status and open research challenges," *IEEE Open J. Commun. Soc.*, vol. 1, pp. 179–189, 2020.

[6] M. S. Ali, H. Tabassum, and E. Hossain, "Dynamic user clustering and power allocation for uplink and downlink non-orthogonal multiple access (NOMA) systems," *IEEE Access*, vol. 4, pp. 6325–6343, 2016.

[7] H. Pan, L. Lu, and S. C. Liew, "Practical power-balanced non-orthogonal multiple access," *IEEE J. Sel. Areas Commun.*, vol. 35, no. 10, pp. 2312–2327, Oct. 2017.

[8] F. Liu, C. Masouros, A. P. Petropulu, H. Griffiths, and L. Hanzo, "Joint radar and communication design: Applications, state-of-the-art, and the road ahead," *IEEE Trans. Commun.*, vol. 68, no. 6, pp. 3834–3862, Jun. 2020.

[9] M. Z. Chowdhury, M. Shahjalal, S. Ahmed, and Y. M. Jang, "6G wireless communication systems: Applications, requirements, technologies, challenges, and research directions," *IEEE Open J. Commun. Soc.*, vol. 1, pp. 957–975, 2020.

[10] A. Bourdoux *et al.*, "6G white paper on localization and sensing," 2020. [Online]. Available: arXiv:2006.01779.

[11] T. X. Han and C. da Silva. *IEEE p802.11—WLAN Sensing (SENS) Study Group (SG)—Meeting Update*, Accessed: Jul. 2020. [Online]. Available: https://www.ieee802.org/11/Reports/senstig_update.htm

[12] M. L. Rahman *et al.*, "Enabling joint communication and radio sensing in mobile networks—A survey," 2020. [Online]. Available: arXiv:2006.07559.

[13] P. Kumari, S. A. Vorobyov, and R. W. Heath, "Adaptive virtual waveform design for millimeter-wave joint communication—Radar," *IEEE Trans. Signal Process.*, vol. 68, pp. 715–730, Nov. 2019. doi: 10.1109/TSP.2019.2956689.

[14] B. Paul, A. R. Chiriyath, and D. W. Bliss, "Survey of RF communications and sensing convergence research," *IEEE Access*, vol. 5, pp. 252–270, 2017.

[15] D. Lopez-Perez, A. Garcia-Rodriguez, L. Galati-Giordano, M. Kasslin, and K. Doppler, "IEEE 802.11be extremely high throughput: The next generation of Wi-Fi technology beyond 802.11ax," *IEEE Commun. Mag.*, vol. 57, no. 9, pp. 113–119, Sep. 2019.

[16] J. Tan, S. Xiao, S. Han, Y. Liang, and V. C. M. Leung, "QoS-aware user association and resource allocation in LAA-LTE/WiFi coexistence systems," *IEEE Trans. Wireless Commun.*, vol. 18, no. 4, pp. 2415–2430, Apr. 2019.

[17] M. M. Şahin and H. Arslan, "Waveform-domain NOMA: The future of multiple access," in *Proc. IEEE Int. Conf. Commun. Workshops (ICC Workshops)*, 2020, pp. 1–6.

[18] M. M. Şahin and H. Arslan, "Multi-functional coexistence of radar-sensing and communication waveforms," in *Proc. IEEE 92nd Veh. Technol. Conf. (VTC-Fall)*, 2020, pp. 1–5.

[19] C. D. Ozkaptan, E. Ekici, O. Altintas, and C. Wang, "OFDM pilot-based radar for joint vehicular communication and radar systems," in *Proc. IEEE Veh. Netw. Conf. (VNC)*, Dec. 2018, pp. 1–8.

[20] M. B. Çelebi and H. Arslan, "Theoretical analysis of the co-existence of LTE-A signals and design of an ML-SIC receiver," *IEEE Trans. Wireless Commun.*, vol. 14, no. 8, pp. 4626–4639, Aug. 2015.

[21] A. Maatouk, E. Çalşkan, M. Koca, M. Assaad, G. Gui, and H. Sari, "Frequency-domain NOMA with two sets of orthogonal signal waveforms," *IEEE Commun. Lett.*, vol. 22, no. 5, pp. 906–909, May 2018.

[22] Z. Ding, R. Schober, P. Fan, and H. V. Poor, "OTFS-NOMA: An efficient approach for exploiting heterogenous user mobility profiles," *IEEE Trans. Commun.*, vol. 67, no. 11, pp. 7950–7965, Nov. 2019.

[23] A. Tusha, S. Doğan, and H. Arslan, "A hybrid downlink NOMA with OFDM and OFDM-IM for beyond 5G wireless networks," *IEEE Signal Process. Lett.*, vol. 27, pp. 491–495, Mar. 2020. doi:10.1109/LSP.2020.2979059.

[24] S. Doğan, A. Tusha, and H. Arslan, "NOMA with index modulation for uplink URLLC through grant-free access," *IEEE J. Sel. Topics Signal Process.*, vol. 13, no. 6, pp. 1249–1257, Oct. 2019.

[25] E. Basar, M. Wen, R. Mesleh, M. D. Renzo, Y. Xiao, and H. Haas, "Index modulation techniques for next-generation wireless networks," *IEEE Access*, vol. 5, pp. 16693–16746, 2017.

[26] A. T. Abusabah and H. Arslan, "NOMA for multinumerology OFDM systems," *Wireless Commun. Mobile Comput.*, vol. 2018, no. 8, Aug. 2018, Art. no. 8514314.

[27] E. Çatak, F. Tekçe, O. Dizdar, and L. Durak-Ata, "Multi-user shared access in massive machine-type communication systems via superimposed waveforms," *Phys. Commun.*, vol. 37, Dec. 2019, Art. no. 100896.

[28] A. Sahin, I. Guvenc, and H. Arslan, "A survey on multicarrier communications: Prototype filters, lattice structures, and implementation aspects," *IEEE Commun. Surveys Tuts.*, vol. 16, no. 3, pp. 1312–1338, 3rd Quart., 2014.

[29] Z. Ding, "Robust beamforming design for OTFS-NOMA," *IEEE Open J. Commun. Soc.*, vol. 1, pp. 33–40, 2020.

[30] E. Arslan, A. T. Dogukan, and E. Basar, "Index modulation-based flexible non-orthogonal multiple access," *IEEE Wireless Commun. Lett.*, vol. 9, no. 11, pp. 1942–1946, Nov. 2020.

[31] M. B. Shahab, S. J. Johnson, M. Shirvanimoghaddam, M. Chafii, E. Basar, and M. Dohler, "Index modulation aided uplink NOMA for massive machine type communications," *IEEE Wireless Commun. Lett.*, vol. 9, no. 12, pp. 2159–2162, Dec. 2020.

[32] M. Vaezi, H. V. Poor, and Z. Ding, *Multiple Access Techniques for 5G Wireless Networks and Beyond*. Heidelberg, Germany: Springer, 2019.

[33] M. Al-Imari, P. Xiao, M. A. Imran, and R. Tafazolli, "Uplink non-orthogonal multiple access for 5G wireless networks," in *Proc. 11th Int. Symp. Wireless Commun. Syst.*, Aug. 2014, pp. 781–785.
[34] E. Basar, Ü. Aygölü, E. Panayirci, and H. V. Poor, "Orthogonal frequency division multiplexing with index modulation," *IEEE Trans. Signal Process.*, vol. 61, no. 22, pp. 5536–5549, Nov. 2013.
[35] M. Wen, X. Cheng, M. Ma, B. Jiao, and H. V. Poor, "On the achievable rate of OFDM with index modulation," *IEEE Trans. Signal Process.*, vol. 64, no. 8, pp. 1919–1932, Apr. 2016.
[36] G. Caire, G. Taricco, and E. Biglieri, "Bit-interleaved coded modulation," *IEEE Trans. Inf. Theory*, vol. 44, no. 3, pp. 927–946, May 1998.
[37] N. C. Luong, X. Lu, D. T. Hoang, D. Niyato, and D. I. Kim, "Radio resource management in joint radar and communication: A comprehensive survey," 2020. [Online]. Available: arXiv.abs/2007.13146.
[38] L. Zheng, M. Lops, Y. C. Eldar, and X. Wang, "Radar and communication coexistence: An overview: A review of recent methods," *IEEE Signal Process. Mag.*, vol. 36, no. 5, pp. 85–99, Sep. 2019.
[39] M. A. Richards, *Fundamentals of Radar Signal Processing*. Chicago, IL, USA: McGraw-Hill, 2014.
[40] Y. Li and G. L. Stüber, *Orthogonal Frequency Division Multiplexing for Wireless Communications*. New York, NY, USA: Springer, 2011.
[41] F. Hlawatsch and G. Matz, *Wireless Communications Over Rapidly Time-Varying Channels*. Amsterdam, The Netherlands: Elsevier, 2011.
[42] H. Arslan and G. E. Bottomley, "Channel estimation in narrowband wireless communication systems," *Wireless Commun. Mobile Comput.*, vol. 1, no. 2, pp. 201–219, 2001.
[43] M. K. Ozdemir and H. Arslan, "Channel estimation for wireless OFDM systems," *IEEE Commun. Surveys Tuts.*, vol. 9, no. 2, pp. 18–48, 2nd Quart., 2007.
[44] *NR; Physical Channels and Modulation, Version 15.0.0*, 3GPP Standard TS 38.211, Jan. 2018. [Online]. Available: http://www.3gpp.org/DynaReport/38211.htm

MEHMET MERT ŞAHIN (Graduate Student Member, IEEE) received the B.S. degree from Bilkent University, Ankara, Turkey, in 2019. He is currently pursuing the M.S. degree with the University of South Florida, Tampa, FL, USA. He worked with Aselsan Inc. as a Wireless Communication Design Engineer in 2019. His research interests include waveform design, wireless communication, and joint radar sensing and communication.

HÜSEYIN ARSLAN (Fellow, IEEE) received the B.S. degree from Middle East Technical University, Ankara, Turkey, in 1992, and the M.S. and Ph.D. degrees from Southern Methodist University, Dallas, TX, USA, in 1994 and 1998, respectively. From 1998 to 2002, he was with the Research Group, Ericsson Inc., Raleigh, NC, USA, where he was involved with several projects related to 2G and 3G wireless communication systems. Since 2002, he has been with the Electrical Engineering Department, University of South Florida, Tampa, FL, USA. He has also been the Dean of the College of Engineering and Natural Sciences, Istanbul Medipol University since 2014. He was a part-time Consultant for various companies and institutions, including Anritsu Company, Morgan Hill, CA, USA, and the Scientific and Technological Research Council of Turkey (TÜBİTAK). His research interests include physical-layer security, mmWave communications, small cells, multicarrier wireless technologies, co-existence issues on heterogeneous networks, aeronautical (high-altitude platform) communications, and *in vivo* channel modeling.